7

Multidimensional Solitons: Theory

L.D. Carr and J. Brand

7.1 Introduction

The one-dimensional solitons described in Parts II and III of this book can be extended into two and three dimensions. Such extensions are generally unstable [1]. However, in the tightly confined geometries associated with trapped Bose–Einstein condensates (BECs) both bright and dark solitons extended into two and three dimensions can be stabilized for times longer than the lifetime of experiments [2–4]. BECs offer the opportunity to tune a matter-wave gradually from one to two and to three dimensions [5, 6]. In the crossover regimes, new nonlinear objects can appear, such as the *svortex*, a solitary wave which is a soliton-vortex hybrid [7, 8]. The general question of crossover dimensions is an intriguing one in physics.

We will consider both the stable and unstable regimes of higher dimensional solitons, treating such objects theoretically but with an eye towards BEC experiments. BECs are typically contained in harmonic traps, and have a profile ranging from Gaussian to inverse parabolic (cf. the Thomas–Fermi limit in Sect. 4.3 of Chap. 1), depending on the interaction strength [5]. They span tens to hundreds of microns. Their lifetime is on the order of one to a hundred seconds. Both thermal and quantum fluctuations can play a significant role in their dynamics [5]. We must take into account all of these factors when discussing solitons. Moreover, the finite non-uniform nature of trapped BECs leads to significantly different nonlinear dynamics than that found in the GPE for uniform media. To cite a simple example, even in one dimension with periodic boundary conditions the finite domain of the condensate leads to spontaneous symmetry breaking and quantum phase transitions [9, 10].

There are also solitons which do not have a 1D analog. For instance, a vortex–anti-vortex pair in 2D is a solitary wave as it represents a localized excitation which moves coherently [11]. An example in 3D is a vortex ring [12–14]. More complicated topological solitons, such as skyrmions, are possible in multi-component condensates [15]. We will discuss such solitons as

well. It is worth noting that some of these scenaria have also been addressed in the context of nonlinear optics [16].

In keeping with the theme of this book, we will deal mathematically only with the mean-field theory of BECs, described by the Gross–Pitaevskii Equation (GPE), and linear perturbations of the mean field, described by the Bogoliubov–de-Gennes equations (BDGE), see Sect. 4 of Chap. 1. The GPE and BDGE can be derived rigorously from first principles from a second quantized quantum field theory for binary interactions between atoms in a dilute weakly interacting Bose gas well below the critical temperature for Bose–Einstein condensation, as discussed in Chap. 1 and the references therein. We note that there are significant subtleties in interpretation of BDGE solutions; see the appendix of [17] for a discussion of these issues. The GPE plus BDGE picture has an excellent interpretation in terms of quantum fluid dynamics, as discussed by Fetter and Svidzinsky [18].

Lastly, we note that the majority of higher-dimensional results, particularly for non-uniform trapped BECs, are achieved numerically. Many excellent references in computational science describe rigorous numerical methods for the GPE and BDGE (e.g. [19] and references therein). Due to the paucity of exact analytical results, we focus primarily on a coherent summary of numerical studies.

We introduce a small set of notation before proceeding. The effective nonlinearity is given by $g_{\rm eff} = gN$, which can be obtained by a simple rescaling of the wavefunction amplitude. Then the wavefunction $\Psi(\boldsymbol{r}, t)$ is normalized to unity. An axisymmetric harmonic trap can be characterized by its asymmetry parameter $\lambda \equiv \omega_z/\omega_r$, where ω_r is the radial trapping frequency and ω_z the axial trapping frequency. The harmonic oscillator lengths are given by $\ell_z \equiv \sqrt{\hbar/m\omega_z}$ and $\ell_r \equiv \sqrt{\hbar/m\omega_r}$.

7.2 Dark Solitons and Solitary Waves in Higher Dimensions

7.2.1 Dark Band and Planar Solitons

In a three dimensional system a standing dark soliton takes the form of a planar node; in two dimensions the node is a line, sometimes called a band. When such a soliton moves with respect to the background condensate, the notch fills in, so that the density in the region of the soliton is reduced but does not form a node; a detailed description is provided in Part III. We term these *planar solitons* and *band solitons*, respectively. In uniform media it is well known that both planar and band solitons decay via the snake instability. A sinusoidal mode transverse to the plane/band grows exponentially. The arcs of this "snake" break off into vortex–anti-vortex pairs. In the context of Bose–Einstein condensates, this has actually been suggested as a way to produce

both vortices and anti-vortices in the same condensate, which is not otherwise possible with the usual stirring techniques.

The decay time for band solitons has been calculated with the BDGE, i.e., by considering linear perturbations to band/planar dark soliton stationary state of the GPE [20, 21]. *Nonlinear* instability times can be significantly shorter, and are determined from the numerical integration of the GPE. A band soliton then decays into an infinite chain of vortex anti-vortex pairs. Depending on the initial condition, these pairs can join to form solitary waves or annihilate in vortex–anti-vortex collisions.

The nonlinear dynamics following decay of a planar soliton can be significantly more complex, as linear excitations leading to the snake instability can occur in two dimensions. The vortices produced are vortex lines which can rotate and/or combine to form vortex rings [22]. Keeping in mind that a velocity field can equally well be characterized by a vorticity field under certain simple assumptions [13], the decay of large arrays of planar vortices can lead to turbulence, characterized by densely tangled vortex lines [23, 24].

In trapped BECs the situation is quite different. In the three-dimensional harmonic trap the condensate, for sufficiently large nonlinearity, has a central parabolic profile and Gaussian tails. In this regime, called the *Thomas–Fermi regime*, as defined in Sect. 4 of Chap. 1, there is an additional mechanism for instability. Since a planar soliton moves at a fraction of the sound velocity which depends on its depth, and the sound velocity is proportional to the square root of density [5], the non-uniform density profile causes the soliton to travel more slowly at the edges of the condensate than the center. An initially uniform planar soliton formed in the center of the trap deforms into a U-shaped propagation front. When this wavefront reaches the edge of the trap it is deflected, and the trailing edges curl up to form vortices [25]. Thus there are two competing instability mechanisms for planar dark solitons in BECs. In initial experiments on planar solitons, it was in fact the non-uniformity-induced instability which dominated, as discussed in Chap. 8. Here, we emphasize the snake instability.

Shown in Fig. 7.1 (reproduced with permission of the authors [4]) are the precise dynamics of the snake instability in a harmonic trap for an initially stationary planar soliton with realistic experimental parameters. In Fig. 1(a) the condensate contains 10^5 atoms and is in a spherical trap with $\omega_r = \omega_z = 2\pi \times 50$ rad/s. The initial single planar soliton state is obtained with imaginary time relaxation. Shown in the panels are snapshots after real time propagation of 47, 50, and 77 ms for Fig. 1(a)(i)–(iii) and (iv)–(vi). In (i)–(iii), the brightness is proportional to the condensate density, and the images correspond to densities integrated down the line of sight. In (iv)–(vi), the brightness is *inversely* proportional to the condensate density, and regions outside the Thomas–Fermi sphere are rendered transparent in order to visualize nodes in the condensate interior; the color corresponds to the phase: $\phi = 0$ through 2π is represented by the sequence red–green–blue–red. The view is perpendicular

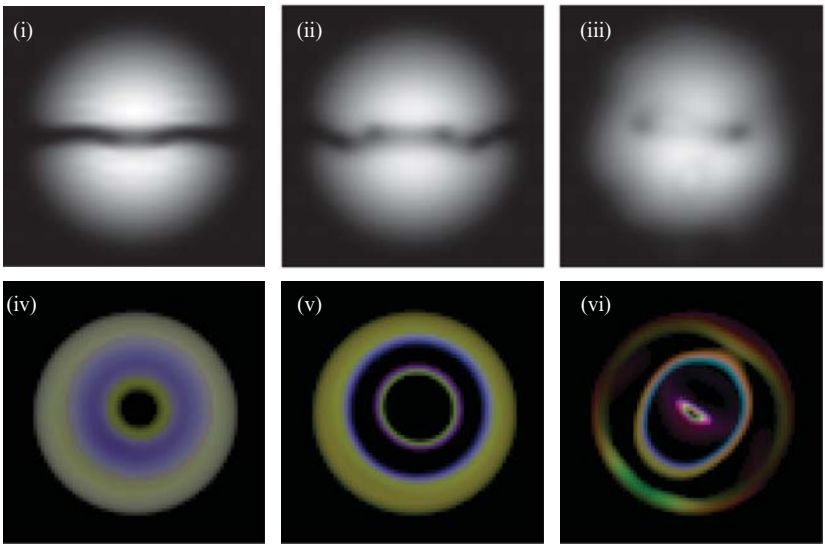

(a) Snake instability in a spherical trap

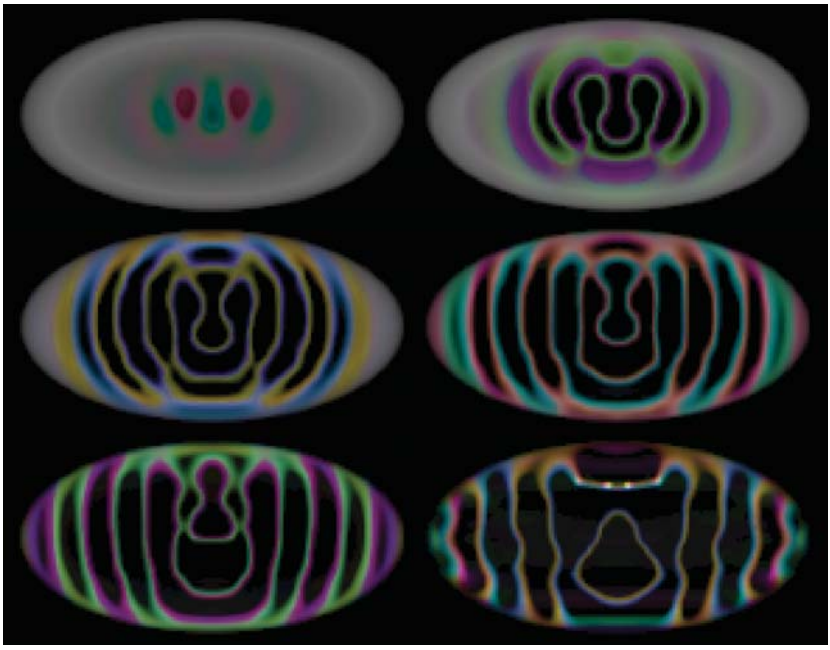

(b) Snake instability in a non-axisymmetric trap

Fig. 7.1. Dynamical instability of a single planar soliton in a trapped Bose–Einstein condensates. See text for full description

to the original nodal plane of the soliton; prior to the snake instability the dark soliton would appear as a featureless disk.

In Fig. 1(b) the breakup of an initial planar soliton is shown as a function of time for $N = 10^6$ atoms, $\omega_x = 2\pi \times 14$ rad/s, $\omega_y/\omega_x = \sqrt{2}$, and $\omega_z/\omega_x = 2$, the precise geometry of [25]. From the top left to the bottom right in raster order are shown times $t = 15$–20 ms in 1 ms increments after the initial state is formed. The view is along $\hat{y}$, and the Hamiltonian was constrained to even parity along $\hat{x}$ and $\hat{z}$ for ease of computation. The rendering is identical to that of Figs. 1(a)(iv)–(vi). The filamentation is almost entirely constrained to the original nodal (x, z)-plane.

These figures describe only the mean-field picture. Recent studies have shown that finite temperature can cause significant dissipative effects even in one dimension [26, 27], while coupling to transverse modes can lead to dissipation within the GPE/BDGE picture [28]. Moreover, even in one dimension quantum fluctuations determined by the BDGE "blur" a dark soliton, due to uncertainty in the position of the density minimum [29]. A full theory of dark band and planar soliton dynamics with even lowest order finite temperature and quantum effects remains a significant challenge to the computational and theoretical scientific communities, although general theoretical prescriptions in this direction exist [30–32].

7.2.2 Ring Dark Solitons and Spherical Shell Solitons

Another way to create a higher dimensional soliton is to wrap a band or planar soliton back around on itself. In two dimensions this takes the form of a nodal ring, termed a *ring dark soliton*. In three dimensions such an object is a nodal spherical shell, termed a *spherical shell soliton*. These objects are always unstable in harmonic traps, but can have lifetimes longer than that of BEC experiments. Multiple ring solitons can be nested within each other. It is mathematically intriguing that such solutions are *nonlinear Bessel functions*, by which we mean solutions to the equation

$$\eta_q'' + \frac{1}{\chi}\eta_q' - \frac{q^2}{\chi^2}\eta_q - \eta_q^3 + \eta_q = 0\,, \tag{7.1}$$

where the wavefunction has been rescaled as

$$\psi(\boldsymbol{r}, t) = \sqrt{\frac{\mu}{g}}\,\eta_q(\chi)\exp(iq\phi)\exp(-i\mu t/\hbar)\exp(i\theta_0)\,. \tag{7.2}$$

Here μ is the chemical potential, q is the winding number of a central vortex, θ_0 is an arbitrary phase, and the coordinate system is cylindrical with coordinates χ, ϕ, with $\chi \equiv (\sqrt{2m\mu}/\hbar)r$. Equation (7.1) is clearly the generating equation of a Bessel function, modified by the nonlinear term η_q^3.

In infinitely extended repulsive condensates, the solutions to (7.2) include the uniform ground state, singly and multiply-quantized vortices, and ring

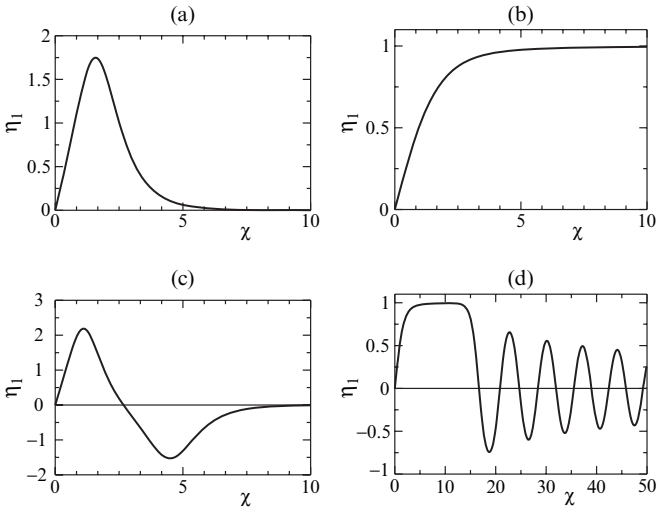

Fig. 7.2. A quantum vortex of winding number $q = 1$ in free space: (**a**) attractive case; (**b**) repulsive case. It is evident in (**a**) that a bright vortex is also a bright ring soliton. A radially excited state: (**c**) the first excited state in the attractive case; (**d**) in the repulsive case, a radially excited state requires an infinite number of nodes and asymptotically resembles the Coulomb function [33]. The radial dependence of the order parameter of an infinitely extended condensate is depicted. Note that all axes are dimensionless: η_1 is a rescaled radial density while χ is a rescaled radial coordinate

soliton solutions, as illustrated in Fig. 7.2b,d. The latter require a countably infinite number of nested dark ring solitons, where each soliton is a radial node corresponding to a node of the nonlinear Bessel function. The asymptotic form of these solutions has been studied in [33].

In contrast, in harmonically trapped condensates, ring solitons can be added to a solution one by one, so that there is a denumerably infinite set of ring soliton solutions for fixed nonlinearity. The linear stability analysis of these solutions and subsequent nonlinear dynamics of their breakup has been studied via the BDGE and GPE in the context of both BECs [33–35] and optics [36–41]. The dominant decay modes of single ring solitons in harmonically trapped BECs with and without a central vortex of winding number unity are the quadrupole and octupole, respectively [33]. In general, instabilities in higher dimensions can lead to new nonlinear structures; in Refs. [34] it is shown that ring solitons decay into vortex necklaces, as was later observed in optics experiments [42]. References [34,35] also provide an analytical description of ring dark soliton dynamics in BECs. It has been suggested that, by use of an optical phase-shifting technique such as that employed in creating planar solitons [25,26,43], one might be able to generate ring solitons in experiments on BECs and observe their subsequent dynamics.

We note that structures similar to those of the stationary spherical shell solitons have been observed as transients in an experiment by Ginsberg et al. [44] and in simulated collisions of vortex rings [45] as will be discussed in Sect. 7.2.3 and Chap. 8.

7.2.3 Solitary Waves in Restricted Geometries

When a condensate is confined to a strongly prolate harmonic trap such that its transverse dimensions are not so small as to approach the healing length but not so large as to be effectively three-dimensional, new families of solitary waves arise. It suffices to consider the case $\omega_z = 0$, $\omega_r \neq 0$, so that the condensate forms an infinitely long cylinder. Physically, one can loosely interpret this as a multi-mode waveguide, where a uniform condensate forms the "vacuum" and solitary waves can propagate in the z direction. In this picture, one maintains a finite linear particle density $n_1 = N/L$, counting the number of particles per unit length along the symmetry axis z.

A mathematical representation of this geometry is realized by the GPE in the following dimensionless form:

$$\mathrm{i}\,\frac{\partial \Psi}{\partial t} = -\frac{1}{2}\,\nabla^2 \Psi + \frac{1}{2}\,r^2\,\Psi + 4\pi\gamma\,|\Psi|^2 \Psi, \tag{7.3}$$

where $r = \sqrt{x^2 + y^2}$ is the radial coordinate and $\nabla^2 = \partial^2/\partial x^2 + \partial^2/\partial y^2 + \partial^2/\partial z^2$ is the Laplacian operator [46]. The dimensionless coupling constant $\gamma \equiv n_1 a$ is the only parameter entering the equation, where a is the scattering length. Length is measured in units of the transverse oscillator length ℓ_r and the unit of time is $1/\omega_r$. At $z \to \pm\infty$ the wave function approaches the ground state in the transverse plane with $\partial\Psi/\partial z = 0$ and a transverse normalization of $2\pi \int \mathrm{d}r\, r|\Psi|^2 = 1$.

The parameter γ characterizes the dimensionality of the problem (see Sect. 3 in Chap. 1 for more details on this reduction). In fact, γ is closely related to the number of healing lengths that fit into the transverse diameter of the cylindrical BEC cloud. Consequently, $\gamma \ll 1$ corresponds to the one-dimensional regime, where the transverse profile of the density is Gaussian and the waveguide is single-mode. In this regime, the only solitary waves known are the familiar family of dark solitons from the one-dimensional NLS. Three-dimensional aspects only become relevant when we consider effects that are sensitive to the breaking of integrability in the system as it has been found, e.g., in the interactions of phonons with solitons [47]. For $\gamma \gg 1$, the condensate enters the Thomas–Fermi regime for which the transverse density profile is approximated by an inverted parabola (cf. Sect. 4 in Chap. 1). In this regime various families of solitary waves with different structures co-exist. Figure 7.3 shows a schematic of possible configurations.

Families of cylindrically symmetric solitary waves have been numerically characterized by Komineas and Papanicolaou [22, 46, 49] and consist

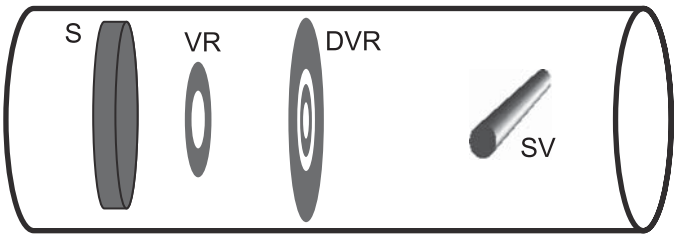

Fig. 7.3. Schematic of solitary wave configurations in a cylindrical BEC. The band soliton (S) has a nodal plane perpendicular to the trap axis and shows axial and inversion symmetry. The vortex ring (VR) is axisymmetric and has a vortex line (line singularity in the phase) in the configuration of a closed ring around the trap axis. The double vortex ring (DVR) has the same symmetries as the VR but features two concentric loops of vortex lines. The solitonic vortex (SV) has no symmetry. A vortex line is configured perpendicular to the trap axis and does not close in itself but terminates at the condensate boundaries

of dark solitons, vortex rings and double rings (see Fig. 7.3). The only non-axisymmetric solitary wave discovered so far is the solitonic vortex, or svortex [7], which consists of a vortex line perpendicular to the cylinder axis. This nonlinear excitation has solitonic properties in that it is a stable solitary wave which propagates coherently, and can be generated by stirring in toroidal traps or by spontaneous decay from an unstable band soliton [7, 8]. The dispersion relation of the svortex was calculated for a cylindrical geometry in [48], as shown in Fig. 7.4 (reproduced with permission of the authors [48]).

The picture that emerges from the numerical calculations is the following. For $\gamma < 1.5$ the situation is quasi-one-dimensional and only one solitary wave with the essential properties and structure of the 1D dark soliton exists. For $\gamma > 1.5$ there is a bifurcation and the non-axisymmetric svortex excitation coexists with axisymmetric solitary waves, i.e., band solitons. For $\gamma > 4$, there is another bifurcation and vortex rings coexist with band solitons and svortices. For even larger γ more bifurcations can be expected leading to a "zoo" of solitary waves. Numerical calculations up to $\gamma = 20$ have been performed in [48, 49]. The stability properties of these families of solitary waves have not been studied in detail, although svortices and vortex rings are believed to be dynamically stable.

The stability of vortex rings in particular has been tested numerically by simulating head-on collisions [45], as shown in Fig. 7.5. It was found that vortex rings collide elastically at large and small velocities while dramatically violent collisions occur at intermediate velocities. While these results could be explained in terms of the known dispersion diagrams like Fig. 7.4, a peculiar observation from the simulations was that inelastic collisions can generate shell structures of nearly spherical symmetry reminiscent of the spherical shell solitons discussed in Sect. 7.2.2. Similar structures were also observed in the experiment of [44], which will be discussed in more detail in Chap. 8.

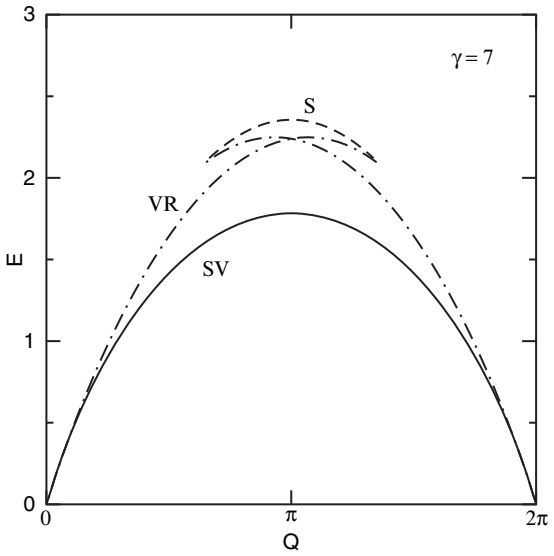

Fig. 7.4. The energy E versus impulse Q dispersion relation of the known solitary waves in the cylindrical BEC at $\gamma = 7$ from [48]. Shown are the branches of the svortex (SV), vortex rings (VR), and the band soliton (S). The slope $\mathrm{d}E/\mathrm{d}Q$ of the dispersion relation gives the velocity of the solitary wave. The density structure of vortex rings and the time-dynamics of their head-on collision is shown in Fig. 7.5

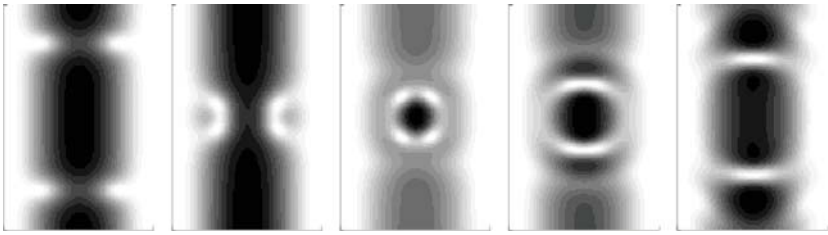

Fig. 7.5. Inelastic collision of vortex rings produces a transient shell structure of near spherical symmetry, from [45]. Plotted is the density $|\Psi|^2$ on the $y = 0$ plane at different time frames showing the head-on collision of a pair of vortex rings at $\gamma = 7$ with $v \equiv \mathrm{d}E/\mathrm{d}Q = 0.34v_\mathrm{s}$, where $v_\mathrm{s} = 1.61$ is the speed of sound in the units of (7.3)

7.2.4 Vortex Rings and Rarefaction Pulses

We now turn to the discussion of solitary waves that are localized on a significantly smaller scale than the condensate dimensions. In this case the idealization to a homogeneous condensate is appropriate, and the local density approximation can be applied to obtain non-uniform results. In fact, most of the work done in this direction assumes an infinite and homogeneous

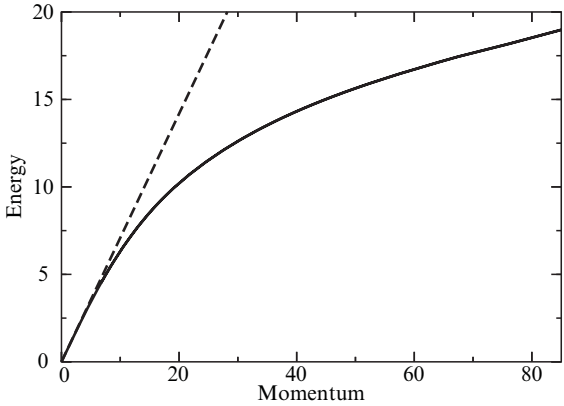

Fig. 7.6. Dispersion relation [11, 51] for 2D (x, z) solitary waves (*solid line*). The *dashed line* shows the dispersion relation of sound for comparison

background density. The ground-breaking work in this area was done in the 1980s by Jones and Roberts, who computed the dispersion relation of 2D and 3D solitary waves [11], as reproduced in Fig. 7.6 [51]. In three dimensions, the solitary waves they found are a family of vortex rings with varying diameter, which is related to the energy, the impulse, and the velocity. As the diameter is decreased to the order of the healing length, the phase singularity disappears; nevertheless, a branch of solitary waves can be found. As these waves have reduced particle density in the region where they are localized, they are also called *rarefaction pulses*. Analytical formulas in the form of Padé approximants for 3D solitary waves are given in [52].

The stability of the Jones–Roberts solitons was first discussed in [53], but rigorous results were only obtained recently [50, 54]. It is interesting to note that simulations showed that head-on collisions of vortex rings are always highly inelastic [55], in contrast to the situation in cylindrical traps discussed above. There has also been some work on the interactions between 3D solitons, vortex lines, and phonon radiation in the context of superfluid turbulence [50, 56]. Recent work in a hydrodynamic framework hints that the properties of vortex rings can be dramatically modified by Kelvin-wave excitations to the extent that the vortex rings may change their direction of propagation [57].

Another specific sort of multidimensional soliton is a solitary wave moving along a vortex line that extends through a homogeneous condensate. Such excitations were discussed recently in [58].

7.2.5 Multi-Component Bose–Einstein Condensates

Multi-component condensates offer rich opportunities for the study of solitonic and solitary waves in higher dimensions. A great deal of work has been done in this area. We touch very briefly on this subject. The main idea

behind topological solitons in multi-component BECs is as follows. Repulsive inter-species and intra-species interactions in a multi-component BEC will tend to make the total particle density uniform by filling up low-density regions of vortex cores with particles from another component. Under the assumption of a uniform total density, the vectorial order parameter has a prescribed constant length and becomes a mapping of three-dimensional real space to a sphere. Topological solitons are found as solutions with nontrivial topology resulting from this mapping. Examples of topological solitons are skyrmions in three dimensions and baby-skyrmions in two dimensions. A very large number of different vortex textures are possible in multi-component BECs [15, 59–61], Various suggestions have been made to observe skyrmions and other such objects in BECs, but none have been achieved so far in experiments [62–69]. There is an ongoing discussion about the potential stability and experimental observability of such solutions [70]. In the case of dipolar BECs where long-range interactions play a role in addition to the contact interaction considered so far, spin textures may form spontaneously and the stability conditions change [71].

We would also like to mention that a generalization of the Jones–Roberts solitons to two-component condensates with a variety of different solitary wave families is described in [72]. Nonlinear phenomena in multi-component BECs are discussed in more detail in Part IX.

7.3 Bright Solitons in Higher Dimensions

While dark solitons are excitations of a condensate that take the form of density notches, bright solitons are ground or metastable states of a condensate, even in higher dimensions. Thus an attractive BEC is *itself* a soliton. Most experiments have focused on the unstable regimes of bright solitons [73–75]; we will also discuss the many theoretical proposals based on stable regimes, which are only just beginning to be explored in experiments [76–78].

7.3.1 Instability, Metastability, Stability

Bright soliton solutions to the GPE with a constant external potential $V(\boldsymbol{r}) = V_0$ are unstable to collapse in three dimensions. In one dimension bright solitons are stable. In two dimensions they either collapse or expand indefinitely, depending on the initial conditions and the strength of the effective nonlinear coefficient. The precise balance between expansion and collapse is known as the Townes soliton, or Townes profile [80, 81]. These now standard results for a constant potential in one, two, and three dimensions are presented rigorously in Sulem and Sulem [1]. However, with the addition of an external harmonic trapping potential, metastability can be achieved in three dimensions. This is easy to see by considering the scaling of the three energy terms in the GPE. The kinetic energy scales as $1/R^2$, where R is the

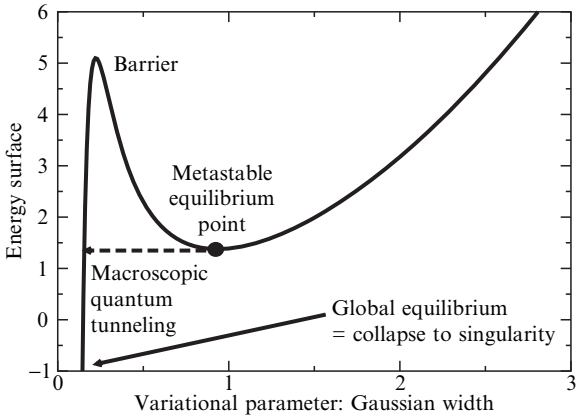

Fig. 7.7. *Metastability and macroscopic quantum tunneling:* Shown is a representative energy surface for a variational Gaussian ansatz in an isotropic 3D harmonic trap for attractive interactions $g_{\rm eff} < 0$, as a function of the single variational parameter, the width of the Gaussian. One observes that non-singular solutions (non-zero width) are always metastable. The height of the collapse barrier decreases as $N \to N_{\rm c}$; $N_{\rm c}$ is the critical number of atoms for which the barrier disappears and collapse is driven classically. Macroscopic quantum tunneling towards collapse can also occur through the barrier, as sketched on the plot [79]

radius of a single bright soliton. The mean-field energy scales as $-1/R^3$, since the wavefunction is proportional to $R^{-3/2}$. The potential energy scales as R^2. Thus the additional contribution of the potential leads to a metastable region.

In Fig. 7.7 is shown a simple variational study for the energy surface in the isotropic case, with R taken as a variational parameter for a Gaussian variational ansatz [82–88]. Since the state shown in Fig. 7.7 is metastable, quantum tunneling can cause the solution to tunnel through the barrier towards $R = 0$, i.e., collapse. Ueda and Leggett [79] derived an expression for the tunneling exponent based on a Gaussian variational ansatz:

$$\frac{S^{\rm B}}{\hbar} \simeq 4.58N \left(1 - \frac{N}{N_{\rm c}}\right)^{5/4} \tag{7.4}$$

where the tunneling rate is given by $\Gamma = A \exp(-S^{\rm B}/\hbar)$ and $N_{\rm c}$ is the critical number of atoms past which the condensate loses metastability and becomes unstable to collapse. This is one of many instances in which macroscopic quantum tunneling manifests in BECs, even within the mean-field description [87,89–91]. One must also make careful estimates of thermal fluctuations, which can push the condensate up over the variational barrier. A simple estimate can be made by requiring that the thermal energy $k_B T$ be much less than the difference between the energy of the metastable state and that of the barrier peak, as sketched in Fig 7.7.

The tunneling barrier becomes large for condensates in prolate traps with $\lambda \ll 1$. The soliton then deforms from a spherical shape to an elongated shape. This is a simple experimental signature of the effective dimensionality of the soliton. For oblate traps, i.e., $\lambda \gg 1$, the soliton becomes two dimensional. Then the condensate is either stable or unstable [86] within the radial degrees of freedom. For sufficiently large $|g_{\rm eff}|$ the condensate collapses; for smaller $|g_{\rm eff}|$ its expansion is prevented by the external harmonic potential. The effect of the asymmetry λ has been studied both variationally and via numerical solution of the GPE [86, 87, 92].

However, condensates in trapped BECs are always mathematically metastable to three-dimensional collapse, whether the effective dimensionality be one-, two-, or three-dimensional, due to quantum tunneling. It is simply that the tunneling time associated with three-dimensional collapse becomes exponentially long; indeed, it is so much longer than experimental lifetimes of 1–100 s that it can be ignored. BEC experiments are rife with such metastabilities; for instance, the ground state of the kinds of alkali metal gases used to make BECs is in fact a crystalline solid, and the atomic gas is only in a metastable state, albeit long-lived. In practice, we ignore all metastabilities not relevant to the time scale of measurements, and assign an effective dimensionality to the GPE to describe bright soliton properties.

Ignoring macroscopic quantum tunneling, the threshold for bright soliton collapse can be determined by variational ansatz from the mean-field theory. This has an analytical expression in two special cases, both of interest for BECs. For an isotropic or nearly isotropic condensate [5, 82, 83, 86], the critical number of atoms is

$$N_{\rm c} = 0.6501 \frac{\bar{\ell}}{|a|}, \tag{7.5}$$

where $\bar{\ell} \equiv (\ell_r^2 \ell_z)^{1/3}$ is the geometric mean of the harmonic oscillator lengths. For a condensate which is confined only in the radial direction, $N_{\rm c} = 0.7598\, \ell_r/|a|$ [87]. This case is especially interesting as it corresponds to the propagation of a bright soliton in a waveguide. Since bright solitons are themselves BECs which self-cool to zero temperature [87], they have been suggested as carriers of information in atom circuits on a chip. We note that numerical studies of the GPE show that the actual critical number is shifted by 10–20% as compared to the variational result; this can be incorporated by simply shifting the constant prefactor.

Lastly, although we have focused on the mean-field and its linear perturbations as described by the GPE and BDGE, this picture is inadequate for describing the dynamics of attractive BECs past the collapse threshold. The essential reason is that the density becomes so large that $\sqrt{n|a|^3} \sim 1$, where n is the number density and a the scattering length. The mean-field theory, which relies on a diluteness approximation [5, 6], necessarily breaks down at this point. Nevertheless, a number of attempts have been made to describe collapse dynamics with mean field theories. For instance, some

authors have modified the GPE by adding an effective loss rate due to three-body recombination [84,93,94]. Other authors have considered a generalized time-dependent Hartree–Fock–Bogoliubov (HFB) theory which couples the mean atomic field to a mean molecular field as well as normal and anomalous atomic quantum fluctuations [95,96]. A recent extensive study of Wüster et al. [97] has focused on reproducing the time of onset of collapse found in the experiment of [75] comparing simulations using the GPE, HFB, and the stochastic truncated Wigner approximation method for including the effects of quantum fluctuations. The conclusion of this study was that the effect of quantum fluctuations, as compared to GPE simulations, was small and could not explain the discrepancies between the time scales found in the simulations and the significantly faster collapse times seen in the experiment.

7.3.2 Bright Soliton Engineering: Pulsed Atom Lasers and Other Applications

An area that has only begun to be explored experimentally is the many regimes in which bright solitons are stable. As pointed out in Sect. 7.3.1, bright solitons are always metastable in Bose–Einstein condensates, due to the geometries in which they are made. However, the instability times due to quantum tunneling can be much longer than the lifetime of experiments. All of the "stable" applications of BECs which are discussed in Sections 7.3.2–7.3.5 are therefore technically unstable; however, we use the term *experimental stability* to emphasize that from the point of view of measurement they are stable.

In one of the first experimental demonstrations of a bright soliton, a train of nearly 3D bright solitons was created from an elongated BEC via modulational instability [77], as described in Chap. 2. On the other hand, another experiment published simultaneously [87] produced a single bright soliton with a weakly *expulsive* harmonic potential in the z direction, i.e., a harmonic trap turned upside down; the radial harmonic trap was kept quite strong, so that the soliton propagated down a waveguide. The expulsive potential was then used to push the soliton along and accelerate its dynamics. A combination of these two experimental techniques leads to a *pulsed atom soliton laser* as follows [98]. The large repulsive scattering length of an initially highly elongated BEC is suddenly tuned small and negative with a Feshbach resonance. At the same time, the trap is flipped over in the z direction, i.e., $\omega_z \to \mathrm{i}\omega_z$. The subsequent nonlinear evolution of the wavefunction creates a series of pulses via modulational instability seeded by linear interference fringes according to the Feynman propagator [99]. These self-cooling "mini-BECs" each contain on the order of 10^3 to 10^4 atoms. They are prevented from overlapping, and thereby collapsing, by the expulsive potential, and maintain their phase coherence over 500 ms. This sequence of events is illustrated in Fig. 7.8.

Improvements on this design have since been suggested in which many more laser pulses can be produced from a better controlled reservoir. In [100],

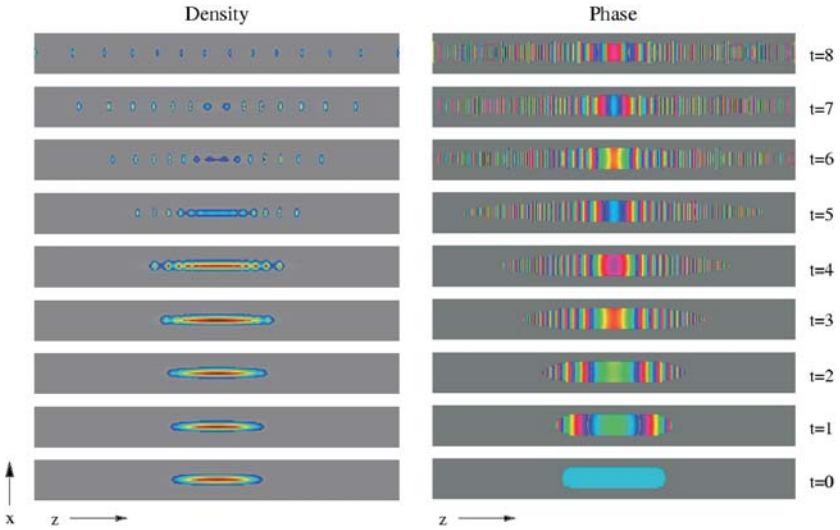

Fig. 7.8. *Pulsed atom soliton laser*: An initial state created by changing the scattering length of a condensate from large and positive to small and negative and then projecting the condensate on to an expulsive harmonic potential results in spontaneous modulational instability and a series of phase-coherent pulses, or "mini-BECs." Shown are the evolution of the density and phase along a two dimensional cut at $y = 0$. A set of well-defined solitonic pulses is evident in the latest (*top*) panel. The strong variations in the phase at late times is due to the high momentum of the solitons caused by the expulsive harmonic potential. Note that the phase is shown on the color circle, i.e., modulo 2π, while the density is in arbitrary relative units rescaled for each plot. For $N = 10^4$ atoms, $a = -3a_0$, and a trap geometry of $\omega_\rho = 2\pi \times 2.44\,\mathrm{kHz}$, $\omega_z = 2\pi\mathrm{i} \times 2.26\,\mathrm{Hz}$, the time units are scaled to 22 ms and the spatial units to $10\,\mu\mathrm{m}$. Note that the aspect ratio of the plots showing a region of 0.822 by 153 length units was changed for visualization

a dual-core approach is used to produce a matter-wave soliton laser from attractive BECs. Two elongated quasi-one-dimensional condensates, or "cores" are laid side by side. The first condensate serves as a reservoir for the second via macroscopic quantum tunneling. The scattering length is small and positive in the first condensate, and small and negative in the second. Bright solitons form in the second condensate, and are emitted through a semi-transparent barrier at one end.

Carpentier and Michinel [101] investigate this idea in much greater detail by considering many possible spatial variations of the scattering length to maximize output and control over pulse size and velocity. In a second paper, they use a similar idea to create a bright soliton accelerator in a ring-shaped trap, similar to the "nevatron" already realized experimentally with repulsive BECs [102], but with many advantages over the first demonstration [103]. A *temporal* variation of the scattering length has also been used to engineer

bright solitons. For instance, a bright soliton in free three-dimensional space can be stabilized by rapidly oscillating the scattering length from positive to negative [104–107].

We would like to point out that even though the "engineering" examples we have cited in this section do not take advantage of the principles of quantum mechanical superposition or entanglement, nevertheless the nonlinear effects which are key to their operation result from averaging over a quantum many body wavefunction. Moreover, quantum fluctuations must be considered in any serious attempt at designing a pulsed atom laser and other such devices. Therefore, they can be considered as examples of quantum engineering.

7.3.3 Solitons in a Thermal Bath

The study of thermal effects on bright matter-wave solitons is highly relevant in light of potential applications of solitons, and has just begun to be explored. The multidimensional aspects of bright solitons in a BEC are very important in this context. The microscopic interactions between solitons and independent thermal particles are described by the BDGE to lowest order in $1/N$, where N is the number of particles in the soliton. In one dimension the scattering problem of a single-particle with a soliton can be solved exactly in the BDGE [108] and the full quantum field theory [109]. It is found that the scattering of thermal particles on the soliton is *reflectionless*, i.e., the transmission coefficient is unity, which is a consequence of the integrable nature of the nonlinear Schrödinger (NLS) equation. This is a very useful property for possible applications of bright solitons in high-precision interferometry.

However, the extent into transverse dimensions that solitons have in a waveguide geometry breaks the integrability of the NLS equation and allows for a finite reflection probability of scattering thermal particles. During such reflection events, momentum is transferred from the thermal particle to the soliton, which affects the soliton's center-of-mass motion. Therefore, a soliton immersed in a thermal cloud can experience diffusive motion or be subject to a frictional force when it is moving with a relative velocity to the background. In [108], the friction and diffusion coefficients were determined based on a calculation of the reflection probability of thermal particles scattering off a soliton. Other approaches to describing the interaction based on the Hartree–Fock–Bogoliubov formalism can potentially treat the nonlinear coupled dynamics of the thermal cloud and the BEC. Studies in this direction are reported in [110, 111].

7.3.4 Soliton–Soliton Interactions

Soliton–soliton interactions in one dimension have been described completely and analytically by Gordon [112]. They are perfectly elastic. However, new features arise in trapped BECs. The imposition of a trapping potential can lead to chaotic dynamics for three or more solitons, even in one dimension [113].

Higher-dimensional effects can lead to inelastic collisions [98, 114, 115]. The subject of collisions of bright solitons in trapped BECs is only just beginning to be studied.

The essential effects of higher dimensionality are as follows. When two identical bright solitons overlap they double their number of atoms N. Thus it is possible for N to be temporarily greater than N_c, as defined in (7.5). The time for collapse to occur can be estimated from g_{eff}. Elasticity is then a question of whether or not the two solitons spend enough time overlapping to undergo collapse or partial collapse, at least within the mean-field picture of the GPE. This is determined by their relative velocity [114]. An additional factor is their relative phase and amplitude. In one dimension, a relative amplitude difference is equivalent to a phase difference [112]. If the phase difference $\Delta\phi$ satisfies $\pi/2 \leq \Delta\phi \leq 3\pi/2$ then the solitons can never overlap. On the other hand, if their phase difference satisfies $-\pi/2 < \Delta\phi < \pi/2$, then partial overlap occurs, with full overlap for $\Delta\phi = 0$ [116]. Initial studies indicate that the situation is vastly more complex in higher dimensions. For example, bright solitons can collide so inelastically that they "stick," releasing excess energy and relative momentum by emitting a few particles, similar to the way that a soliton in one dimension adjusts to its preferred shape and thereby self-cools [87, 117].

It has been suggested, based on initial experiments on bright soliton trains, that bright soliton collisions can in fact lead to annihilation [77]. Beyond the mean-field theory, it is known experimentally that there is a bounce from collapse, as described in Sect. 7.3.1. Consider two solitons in a soliton train, each with a number of atoms near the critical number and therefore nearly three dimensional. The harmonic trap and/or initial conditions can drive them to overlap. If they do so for a sufficient period of time partial collapse occurs, leaving one soliton behind. The loss of atoms is not properly described by the mean-field theory. Even if the solitons are initially arranged with nodes between them, drift of relative phase due to quantum fluctuations can eventually lead to their being able to overlap. This is one explanation of the occasional disappearance of a member of the soliton trains of [77].

Therefore, in addition to the exploration of bright soliton collisions within the three-dimensional mean-field theory of the GPE, the effects of finite temperature [27] and higher order quantum theories [95] need to be considered as well in order to model experimental dynamics. The mean-field theory can only provide, at best, the threshold for collapse-related effects. This remains an important open problem for theorists to address.

7.3.5 Bright Ring Solitons and Quantum Vortices

The attractive analog of a vortex in a repulsive BEC in free space is in fact a bright ring soliton [118]. This point is illustrated in Fig. 7.2, where it can be seen that the wavefunction approaches zero as $r \to \infty$, in contradistinction to vortices in repulsive BECs where the wavefunction approaches a non-zero

constant. The stability of vortices in attractive BECs has been investigated theoretically [82,83,119,120] since shortly after the experimental observation of a BEC. However, no experiment to date has tested theoretical predictions of bright ring solitons.

Static studies, which consider stationary solutions of the GPE and their linear perturbations as described by the BDGE, have found that all bright ring solitons and their radial excitations are unstable [118,120]. Initial studies predicted an enhanced critical number over a bright soliton, and therefore *enhanced* stability. However, these studies considered only radial collapse. In fact, bright ring solitons are azimuthally unstable, as later analysis with the BDGE showed [120]. Although we have avoided significant analytical description thus far in this review, it is useful to state the form of the BDGE for a centrally located axisymmetric vortex [121] in an effectively two-dimensional condensate. We first transform the Bogoliubov amplitudes u and v according to

$$\begin{pmatrix} u(\boldsymbol{r}) \\ v(\boldsymbol{r}) \end{pmatrix} = \frac{\mathrm{e}^{\mathrm{i}m\phi}}{\ell_r} \begin{pmatrix} \mathrm{e}^{\mathrm{i}q\phi}\,\tilde{u}_m(\tilde{r}) \\ \mathrm{e}^{-\mathrm{i}q\phi}\,\tilde{v}_m(\tilde{r}) \end{pmatrix}, \tag{7.6}$$

where $\tilde{r} = \sqrt{x^2+y^2}/\ell_r$ and we neglect perturbations in the z direction, considering only a strongly oblate trap for simplicity. Equation 7.6) represents a partial wave of angular momentum m relative to a condensate with a vortex of winding number q. Then in harmonic oscillator units the BDGE become

$$\mathcal{L}_+\tilde{u}_m - \tilde{g}_{\mathrm{eff}}|\tilde{f}_q|^2\tilde{v}_m = \frac{\Omega_m}{\omega}\tilde{u}_m, \tag{7.7}$$

$$\mathcal{L}_-\tilde{v}_m - \tilde{g}_{\mathrm{eff}}|\tilde{f}_q|^2\tilde{u}_m = -\frac{\Omega_m}{\omega}\tilde{v}_m, \tag{7.8}$$

where

$$\mathcal{L}_\pm \equiv -\frac{1}{2}\left(\frac{\partial^2}{\partial\tilde{r}^2} + \frac{1}{\tilde{r}}\frac{\partial}{\partial\tilde{r}} - \frac{(q\pm m)^2}{\tilde{r}^2} - \tilde{r}^2\right) + 2\tilde{g}_{\mathrm{eff}}|\tilde{f}_m|^2 - \tilde{\mu} \tag{7.9}$$

Here Ω_m are the eigenvalues for Bogoliubov modes with angular momentum m and $\tilde{f}_q$ is the radial portion of condensate wavefunction with winding number q; the tildes throughout these rescaled BDGE indicate harmonic oscillator units. The different centrifugal barriers inherent in $\mathcal{L}_\pm$ show that the two amplitudes behave differently near the origin, with $\tilde{u}_m \propto \tilde{r}^{|m+q|}$ and $\tilde{v}_m \propto \tilde{r}^{|m-q|}$ as $\tilde{r}\to 0$. Note that $\tilde{f}_q$ is normalized to unity.

We briefly highlight the results of studies of (7.7)–(7.8) for $\tilde{g}_{\mathrm{eff}} < 0$. The dominant instability mode is quadrupolar for $m = 1$, a single bright soliton, and small $\tilde{g}_{\mathrm{eff}}$. The linear instability time is given by $T_m = 2\pi/\mathrm{Im}(\Omega_m)$. This time can be much longer than experiments, so that bright ring solitons do indeed have the possibility of being observed.

While multiple dark ring solitons consist of nested nodal rings, separated by regions of nonzero density and constant phase, multiple bright ring solitons consist of multiple rings of non-zero density and constant phase separated by

nodes. These multiple bright ring soliton solutions are in fact radial excitations of a vortex in an attractive BEC. In free space, there is a denumerably infinite number of such states, which form an excited state spectrum of bright ring solitons in two dimensions for fixed winding number under the constraint that the wavefunction approach zero as the radial coordinate approaches infinity. This result has been formally proved for winding number zero for the Townes soliton [1] and numerically demonstrated for non-zero winding number [118]. The first excited state for winding number $m = 1$ is shown in Fig. 7.2c. This is in contrast to dark ring solitons, which only appear in an infinite number of concentric rings in free space, as shown in Fig. 7.2d.

It is has been shown that a similar sequence of radially excited states of attractive vortices occurs in a harmonic trap, and that, for sufficiently small $\tilde{g}_{\rm eff}$, their instability times can be long compared to experiments [118].

Nonlinear dynamical studies of trapped bright ring solitons have found cyclical behavior in their azimuthal break-up, among other intriguing behaviors [122, 123]. Figure 7.9 shows one example of this cyclical behavior. The initial state is a bright ring soliton plus a small symmetry-breaking azimuthal perturbation. The ring splits via the quadrupole instability into two density peaks, i.e., two bright solitons. The soliton pair rotates around the origin, then recombines to reform the original ring. Panels g and h suggest the possibility of observation by sudden switching of the scattering length and expansion

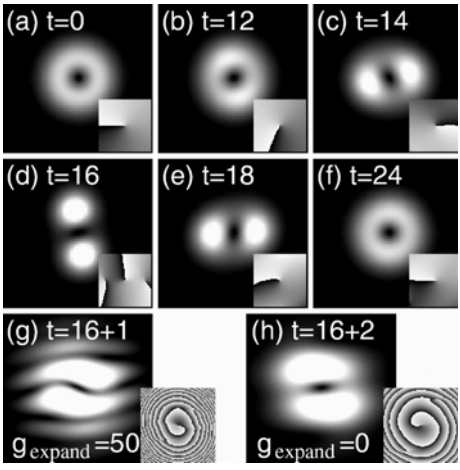

Fig. 7.9. Nonlinear dynamical split-merge cycle of bright ring soliton. (**a**)–(**f**) Shown is the time evolution of the density profile in two dimensions. The insets present gray-scale plots of the phase modulo 2π. Panels (**g**) and (**h**) show what occurs when the trap is switched off and the condensate is allowed to expand with (**g**) large positive scattering length and (**h**) zero scattering length. This is a common experimental technique to magnify condensate features too small to otherwise resolve. Reproduced with permission of the authors [122]

of the condensate, a common experimental technique. We note that parallels have been suggested in multi-component BECs as well [124].

Finally, it is worth mentioning that the stabilization of higher dimensional solitons by means of optical lattices (cf. Parts IV and VIII) has also been proposed in [125–128].

7.4 Summary and Acknowledgments

We have described a few of the many manifestations of soliton-like phenomena in Bose–Einstein condensates in two and three dimensions. A brief list for repulsive nonlinearity includes dark band solitons, dark planar solitons, dark ring solitons, spherical shell solitons, families of solitary waves, and skyrmions and vortex textures; while for attractive nonlinearity one finds metastable bright solitons, quantum tunneling and quantum evaporation of bright solitons, pulsed atom soliton lasers, bright ring solitons, and the split-merge cycle. We think some of the most exciting outstanding problems in this field are the higher order quantum and thermal effects on solitonic phenomena, as we have indicated sporadically throughout our discussion.

There is great deal both in and beyond our over one hundred references that we have been unable to cover in the space allotted; we sincerely hope we have not offended the many investigators whose work we have not been able to include.

The authors would like to thank the editors of this book, who have done a wonderful job facilitating a much-needed review of nonlinear phenomena in BECs. We thank our mentor William Reinhardt, who many years ago led us both in the direction of solitons and BECs as a graduate student and post-doctoral fellow, respectively. LDC thanks Charles Clark for many useful discussions and scientific collaborations which led to writing this chapter. LDC gratefully acknowledges the National Science Foundation for continuing support.

References

1. C. Sulem, P.L. Sulem, *Nonlinear Schrödinger Equations: Self-focusing Instability and Wave Collapse* (Springer, New York, 1999)
2. A.E. Muryshev, H.B. van Linden van den Heuvell, G.V. Shlyapnikov, Phys. Rev. A **60**, R2665 (1999)
3. L.D. Carr, M.A. Leung, W.P. Reinhardt, J. Phys. B **33**, 3983 (2000)
4. D.L. Feder, M.S. Pindzola, L.A. Collins, B.L. Schneider, C.W. Clark, Phys. Rev. A **62**, 053606 (2000)
5. F. Dalfovo, S. Giorgini, L.P. Pitaevskii, S. Stringari, Rev. Mod. Phys. **71**, 463 (1999)
6. A.J. Leggett, Rev. Mod. Phys. **73**, 307 (2001)
7. J. Brand, W.P. Reinhardt, J. Phys. B **34**, L113 (2001)

8. J. Brand, W.P. Reinhardt, Phys. Rev. A **65**, 043612 (2002)
9. L.D. Carr, C.W. Clark, W.P. Reinhardt, Phys. Rev. A **62**, 063611 (2000)
10. R. Kanamoto, H. Saito, M. Ueda, Phys. Rev. Lett. **94**, 090404 (2005)
11. C.A. Jones, P.H. Roberts, J. Phys. A **15**, 2599 (1982)
12. R.J. Donnelly, *Quantized Vortices in Helium II* (Cambridge University Press, New York, 1991)
13. P.G. Saffman, *Vortex Dynamics* (Cambridge University Press, New York, 1992)
14. B.P. Anderson, P.C. Haljan, C.A. Regal, D.L. Feder, L.A. Collins, C.W. Clark, E.A. Cornell, Phys. Rev. Lett. **86**, 2926 (2001)
15. E.J. Mueller, Phys. Rev. A **69**, 033606 (2004)
16. B.A. Malomed, D. Mihalache, F. Wise, L. Torner, J. Opt. B **7**, R53 (2005)
17. L.J. Garay, J.R. Anglin, J.I. Cirac, P. Zoller, Phys. Rev. A **63**, 023611 (2001)
18. A.L. Fetter, A.A. Svidzinsky, J. Phys. **13**, R135 (2001)
19. V.M. Pérez-García, X.Y. Liu, App. Math. Comp. **144**, 215 (2003)
20. C.T. Law, G.A. Swartzlander, Opt. Lett. **18**, 586 (1993)
21. G.S. McDonald, K.S. Syed, W.J. Firth, Opt. Commun. **95**, 281 (1993)
22. S. Komineas, in *Nonlinear Waves in Complex Systems*, ed. by J.G. Caputo, M.P. Soerensen, Eur. Phys. J. Special Topics **147**, 133–152 (2007)
23. K.W. Schwarz, Phys. Rev. B **31**, 5782 (1985)
24. K.W. Schwarz, Phys. Rev. B **38**, 2398 (1988)
25. J. Denschlag, J.E. Simsarian, D.L. Feder, C.W. Clark, L.A. Collins, J. Cubizolles, L. Deng, E.W. Hagley, K. Helmerson, W.P. Reinhardt, S.L. Rolston, B.I. Schneider, W.D. Phillips, Science **287**, 97 (2000)
26. S. Burger, K. Bongs, S. Dettmer, W. Ertmer, K. Sengstock, A. Sanpera, G.V. Shlyapnikov, M. Lewenstein, Phys. Rev. Lett. **83**, 5198 (1999)
27. B. Jackson, C.F. Barenghi, N.P. Proukakis, e-print cond-mat/0610082 (2006)
28. P.O. Fedichev, A.E. Muryshev, G.V. Shlyapnikov, Phys. Rev. A **60**, 3220 (1999)
29. J. Dziarmaga, Z.P. Karkuszewski, K. Sacha, J. Phys. B **36**, 1217 (2003)
30. E. Zaremba, T. Nikuni, A. Griffin, J. Low Temp. Phys. **116**, 277 (1999)
31. S.A. Morgan, Ph.D. thesis, St. John's College, University of Oxford, 1999
32. M.J. Davis, S.A. Morgan, K. Burnett, Phys. Rev. A **66**, 053618 (2002)
33. L.D. Carr, C.W. Clark, Phys. Rev. A **74**, 043613 (2006)
34. G. Theocharis, D.J. Frantzeskakis, P.G. Kevrekidis, B.A. Malomed, Y.S. Kivshar, Phys. Rev. Lett. **90**, 120403 (2003)
35. G. Theocharis, P. Schmelcher, M.K. Oberthaler, P.G. Kevrekidis, D.J. Frantzeskakis, Phys. Rev. A **72**, 023609 (2005)
36. Y.S. Kivshar, X. Yang, Phys. Rev. E **49**, 1657 (1994)
37. W. Dreischuh, A. Fliesser, I. Velchev, S. Dinev, L. Windholz, App. Phys. B **62**, 139 (1996)
38. D. Neshev, A. Dreischuh, V. Kamenov, I. Stefanov, S. Dinev, W. Flieβer, L. Windholz, Appl. Phys. B **64**, 429 (1997)
39. D.J. Frantzeskakis, B.A. Malomed, Phys. Lett. A **264**, 179 (2000)
40. H.E. Nistazakis, D.J. Frantzeskakis, B.A. Malomed, P.G. Kevrekidis, Phys. Lett. A **285**, 157 (2001)
41. A. Dreischuh, D. Neshev, G.G. Paulus, F. Grasbon, H. Walther, Phys. Rev. E **66**, 066611 (2002)
42. J. Yang, I. Makasyuk, P.G. Kevrekidis, H. Martin, B.A. Malomed, D.J. Frantzeskakis, Z. Chen, Phys. Rev. Lett. **94**, 113902 (2005)

43. L.D. Carr, J. Brand, S. Burger, A. Sanpera, Phys. Rev. A **63**, 051601 (2001)
44. N.J. Ginsberg, J. Brand, L.V. Hau, Phys. Rev. Lett. **94**, 040403 (2005)
45. S. Komineas, J. Brand, Phys. Rev. Lett. **95**, 110401 (2005)
46. S. Komineas, N. Papanicolaou, Phys. Rev. Lett. **89**, 070402 (2002)
47. A.E. Muryshev, G. Shlyapnikov, W. Ertmer, K. Sengstock, M. Lewenstein, Phys. Rev. Lett. **89**, 110401 (2002)
48. S. Komineas, N. Papanicolaou, Phys. Rev. A **68**, 043617 (2003)
49. S. Komineas, N. Papanicolaou, Phys. Rev. A **67**, 023615 (2003)
50. N.G. Berloff, J. Phys. A **37**, 1617 (2004)
51. Natalia Berloff provided us with the numerical data used in this figure.
52. N.G. Berloff, J. Phys. A **37**, 1617 (2004)
53. C.A. Jones, S.J. Putterman, P.H. Roberts, J. Phys. A **19**, 2991 (1986)
54. S. Tsuchiya, F. Dalfovo, C. Tozzo, L. Pitaevskii, e-print cond-mat/0607160, (2006)
55. J. Koplik, H. Levine, Phys. Rev. Lett. **76**, 4745 (1996)
56. M. Leadbeater, D.C. Samuels, C.F. Barenghi, C.S. Adams, Phys. Rev. A **67**, 015601 (2003)
57. C.F. Barenghi, R. Hanninen, M. Tsubota, Phys. Rev. E **74**, 046303 (2006)
58. N.G. Berloff, Phys. Rev. A **94**, 010403 (2005)
59. J. Ruostekoski, Phys. Rev. A **70**, 041601 (2004)
60. K. Kasamatsu, M. Tsubota, M. Ueda, Phys. Rev. A **71**, 043611 (2005)
61. W.V. Pogosov, R. Kawate, T. Mizushima, K. Machida, Phys. Rev. A **72**, 063605 (2005)
62. T. Busch, J.R. Anglin, Phys. Rev. A **60**, R2669 (1999)
63. U.A. Khawaja, H. Stoof, Nature **411**, 918 (2001)
64. U.A. Khawaja, H.T.C. Stoof, Phys. Rev. A **64**, 043612 (2001)
65. C.M. Savage, J. Ruostekoski, Phys. Rev. Lett. **91**, 010403 (2003)
66. R.A. Battye, N.R. Cooper, P.M. Sutcliffe, Phys. Rev. Lett. **88**, 080401 (2002)
67. I.F. Herbut, M. Oshikawa, Phys. Rev. Lett. **97**, 080403 (2006)
68. J. Ruostekoski, J.R. Anglin, Phys. Rev. Lett. **86**, 3934 (2001)
69. T. Mizushima, K. Machida, T. Kita, Phys. Rev. Lett. **89**, 030401 (2002)
70. H. Zhai, W.Q. Chen, Z. Xu, L. Chang, Phys. Rev. A **68**, 043602 (2003)
71. S. Yi, H. Pu, Phys. Rev. Lett. **97**, 020401 (2006)
72. N.G. Berloff, Phys. Rev. Lett. **94**, 120401 (2005)
73. C.A. Sackett, H.T.C. Stoof, R.G. Hulet, Phys. Rev. Lett. **80**, 2031 (1998)
74. C.A. Sackett, J.M. Gerton, M. Welling, R.G. Hulet, Phys. Rev. Lett. **82**, 876 (1999)
75. E.A. Donley, N.R. Claussen, S.L. Cornish, J.L. Roberts, E.A. Cornell, C.E. Wieman, Nature **412**, 295 (2001)
76. L. Khaykovich, F. Schreck, F. Ferrari, T. Bourdel, J. Cubizolles, L.D. Carr, Y. Castin, C. Salomon, Science **296**, 1290 (2002)
77. K.E. Strecker, G.B. Partridge, A.G. Truscott, R.G. Hulet, Nature **417**, 150 (2002)
78. S.L. Cornish, S.T. Thompson, C.E. Wieman, Phys. Rev. Lett. **96**, 170401 (2006)
79. M. Ueda, A.J. Leggett, Phys. Rev. Lett. **80**, 1576 (1998)
80. R.Y. Chiao, E. Garmire, C.H. Townes, Phys. Rev. Lett. **13**, 479 (1964)
81. K.D. Moll, A.L. Gaeta, G. Fibich, Phys. Rev. Lett. **90**, 203902 (2003)
82. R.J. Dodd, M. Edwards, C.J. Williams, C.W. Clark, M.J. Holland, P.A. Ruprecht, K. Burnett, Phys. Rev. A **54**, 661 (1996)

83. R.J. Dodd, J. Res. NIST **101**, 545 (1996)
84. Y. Kagan, E.L. Surkiv, G.V. Shlyapnikov, Phys. Rev. Lett. **79**, 2604 (1997)
85. Y. Kagan, E.L. Surkov, G.V. Shlyapnikov, Phys. Rev. A **55**, R18 (1997)
86. V.M. Pérez-García, H. Michinel, J.I. Cirac, M. Lewenstein, P. Zoller, Phys. Rev. A **56**, 1424 (1997)
87. L.D. Carr, Y. Castin, Phys. Rev. A **66**, 063602 (2002)
88. B.A. Malomed, Progr. Optics **43**, 71 (2002)
89. N. Moiseyev, L.D. Carr, B.A. Malomed, Y.B. Band, J. Phys. B **37**, L1 (2004)
90. L.D. Carr, M.J. Holland, B.A. Malomed, J. Phys. B **38**, 3217 (2005)
91. N. Moiseyev, L.S. Cederbaum, Phys. Rev. A **72**, 033605 (2005)
92. A. Gammal, T. Frederico, L. Tomio, Phys. Rev. A **64**, 055602 (2001)
93. H. Saito, M. Ueda, Phys. Rev. A **65**, 033624 (2002)
94. K. Gawryluk, M. Brewczyk, M. Gajda, J. Mostowski, Phys. Rev. B **39**, L1 (2006)
95. J.N. Milstein, C. Menotti, M.J. Holland, New J. Phys. **5**, 52 (2003)
96. S. Wuster, J.J. Hope, C.M. Savage, Phys. Rev. A **71**, 033604 (2005)
97. S. Wüster, B.J. Dabrowska-Wüster, A.S. Bradley, M.J. Davis, P.B. Blakie, J.J. Hope, C.M. Savage, Phys. Rev. A **75**, 043611 (2007)
98. L.D. Carr, J. Brand, Phys. Rev. A **70**, 033607 (2004)
99. L.D. Carr, J. Brand, Phys. Rev. Lett. **92**, 040401 (2004)
100. P.Y. Chen, B.A. Malomed, J. Phys. B **38**, 4221 (2005)
101. A.V. Carpentier, H. Michinel, Europhys. Lett. **78**, 10002 (2007)
102. J.A. Sauer, M.D. Barrett, M.S. Chapman, Phys. Rev. Lett. **87**, 270401 (2001)
103. A.V. Carpentier, H. Michinel, M.I. Rodas-Verde, V.M. Pérez-García, Phys. Rev. A **74**, 013619 (2006)
104. H. Saito, M. Ueda, Phys. Rev. Lett. **90**, 040403 (2003)
105. H. Saito, M. Ueda, Phys. Rev. A **70**, 053610 (2004)
106. S.K. Adhikari, Phys. Rev. A **69**, 063613 (2004)
107. F.K. Abdullaev, J.G. Caputo, R.A. Kraenkel, B.A. Malomed, Phys. Rev. A **67**, 013605 (2003)
108. S. Sinha, A.Y. Cherny, D. Kovrizhin, J. Brand, Phys. Rev. Lett. **96**, 030406 (2006)
109. J.B. McGuire, J. Math. Phys. **5**, 622 (1964)
110. H. Buljan, M. Segev, A. Vardi, Phys. Rev. Lett. **95**, 180401 (2005)
111. I.M. Merhasin, B.A. Malomed, Y.B. Band, Phys. Rev. A **74**, 033614 (2006)
112. J.P. Gordon, Opt. Lett. **8**, 596 (1983)
113. A.D. Martin, C.S. Adams, S.A. Gardiner, Phys. Rev. Lett. **98**, 020402 (2007)
114. N.G. Parker, A.M. Martin, S.L. Cornish, C.S. Adams, e-print cond-mat/0603059 (2006)
115. L. Khaykovich, B.A. Malomed, Phys. Rev. A **74**, 023607 (2006)
116. L.D. Carr, J.N. Kutz, W.P. Reinhardt, Phys. Rev. E **63**, 066604 (2001)
117. J. Satsuma, N. Yajima, Prog. Theor. Phys. (Suppl.) **55**, 284 (1974)
118. L.D. Carr, C.W. Clark, Phys. Rev. Lett. **97**, 010403 (2006)
119. P.A. Ruprecht, M.J. Holland, K. Burnett, M. Edwards, Phys. Rev. A **51**, 4704 (1995)
120. H. Pu, C.K. Law, J.H. Eberly, N.P. Bigelow, Phys. Rev. A **59**, 1533 (1999)
121. A.A. Svidzinsky, A.L. Fetter, Phys. Rev. A **58**, 3168 (1998)
122. H. Saito, M. Ueda, Phys. Rev. Lett. **89**, 190402 (2002)
123. H. Saito, M. Ueda, Phys. Rev. A **69**, 013604 (2004)

124. J.J. García-Ripoll, V.M. Pérez-García, Phys. Rev. Lett. **84**, 4264 (2000)
125. B.B. Baizakov, B.A. Malomed, M. Salerno, Europhys. Lett. **63** 642 (2003)
126. J. Yang, Z.H. Musslimani, Opt. Lett. **28** 2094 (2003)
127. B.B. Baizakov, B.A. Malomed, M. Salerno, Phys. Rev. A **70** 053613 (2004)
128. D. Mihalache, Mazilu, F. Lederer, Y.V. Kartashov, L.-C. Crasovan, L. Torner, Phys. Rev. E **70** 055603(R) (2004)